# Edge-Hydrogenated Germanene by Electrochemical Decalcification-Exfoliation of $CaGe_2$: Germanene-Enabled Vapor Sensor

*Evgeniya Kovalska,* Nikolas Antonatos, Jan Luxa, Zdenek Sofer**

Department of Inorganic Chemistry, University of Chemistry and Technology Prague, Technická 5, 166 28 Prague 6, Czech Republic

**KEYWORDS:** edge-hydrogenated germanene, top-down synthesis, electrochemical exfoliation, vapor sensing.

**ABSTRACT:** Two-dimensional germanene has been recently explored for applications in sensing, catalysis, and energy storage. The potential of this material lies on its graphene-like optoelectronic and chemical properties. However, pure free-standing germanene cannot be found in nature and the synthetic methods are hindering the potentially fascinating properties of germanene. Herein, we report for the first time a single-step synthesis of few-layer germanene by electrochemical exfoliation in non-aqueous environment. As a result of simultaneous decalcification and intercalation of the electrolyte's active ions, we achieved a low-level hydrogenation of germanene that occurs at the edges of the material. The obtained edge-hydrogenated germanene flakes have a lateral size of several micrometers which possess a cubic structure. We have pioneered the potential application of edge-hydrogenated germanene for vapor sensing and demonstrated its specific sensitivity to methanol and ethanol.

We have shown a selective behavior of the germanene-based sensor that appears to increase the electrical resistance in the vapors where methanol prevails. We anticipate that these results can provide a new approach for emerging layered materials with the potential utility in advanced gas sensing.

## INTRODUCTION

In pursuit of novel two-dimensional (2D) materials, scientists are keen to complement graphene's capabilities and overcome challenges induced by its zero-bandgap nature, low intrinsic optical absorption, inapplicability in the Si/Ge-based semiconductor industry as well as low surface reactivity. Recently, 2D allotrope of germanium – germanene – and its modifications, low-buckled analogues of graphene, have attracted considerable attention due to their unique physical and chemical properties. Germanene is a near-planar hexagonal structure with 0.24 and 0.42 nm distances between Ge-Ge atoms and layers, respectively.[1] Free-standing germanene layer was theoretically predicted for the first time in 2009[2] reporting a narrow bandgap opening (about 0.024 eV)[1] in contrast to the zero bandgap of graphene. This promotes a quantum-spin Hall effect[3] and massless Dirac fermions,[4] that together with the tunable bandgap,[5, 6] makes germanene's use realistic for optoelectronics,[7-9] sensing,[10-12] energy storage,[13-15] and catalysis.[6, 16, 17] The electronic and magnetic properties of buckled germanene are size and geometry determined and can be tuned by strain[18, 19] or surface functionalization.[20-22] It is worth noting that germanene stability is low, however, germanene derivates are stable. For example, germanane ("hydrogenated germanene", Ge-H) or methyl germanane ("methyl terminated germanene") are the most stable and studied forms. Nevertheless, it has not been electrochemically exfoliated yet from bulk germanium.[23]

Various attempts to produce germanene have been demonstrated using top-down and bottom-up methods. Recently ultrahigh vacuum (UHV) techniques such as chemical vapor deposition and molecular beam epitaxy, together with high-temperature annealing have been reported to produce germanene. UHV germanene has been grown on various substrates such as Au,[24] Pt,[25] Ag,[26] Al,[27] Si,[28] graphite,[29], and $MoS_2$.[30] Germanene formation is not limited to bottom-up synthesis as shown by the electrochemical deposition of germanene in aqueous,[1, 31-34] and nonaqueous medium.[35-37] However, electrochemical deposition can be self-limited to approximately several germanene layers filled with the defect domains.[34]

It has been known that the synthesis of germanene-based materials by deintercalation of corresponding Zintl phases (e.g., $CaGe_2$, $EuGe_2$)[38, 39] is a commonly used method. For instance, Ge-H was prepared by liquid-phase exfoliation from bulk $CaGe_2$ in concentrated HCl at low temperatures.[39-42] The as-exfoliated samples possess a direct bandgap (1.55 eV) and five times higher carrier mobility in contrast to bulk Ge.[39] Later, the same authors reported methyl functionalized germanene (Ge-Me) by exfoliation in two-phase system $CH_3I/H_2O$; Ge-Me exhibited higher thermal stability compared to germanane and larger bandgap (1.7 eV).[20] Deintercalation of Ca from bulk $CaGe_2$ using inositol hexakisphosphate acid ($IP_6$) was demonstrated to produce germanene sheets; the final product included multiple phases of calcium germanides and Ge-based nanosheet bundles.[43] Several layers of hexagonal germanene by using fluoride diffusion in the $CaGe_2$ crystal have also been reported.[44] The structures were suitable for high-performance electronic systems. Furthermore, a low-energy synthesis of organo- and hydrogen-terminated germanene was proposed using metallic Ge or its oxide form ($GeO_2$).[45] Authors describe recyclable quinone/catechol redox reactions as an

alternative to elemental chlorine/hydrochloric acid in the conversion of Ge and $GeO_2$ to a $GeCl_4$. Nevertheless, these developed methods produce low yield of germanene, they are time-consuming, and complicated in terms of reaction conditions, *e.g.* aggressive acidic medium, and low temperatures.

Herein, for the first time, we demonstrate a single-step synthesis of low hydrogenated germanene (namely, edge-hydrogenated germanene – $H_{edge}$-Ge) by low-potential electrochemical exfoliation of $CaGe_2$ in 0.01 M tetrabutylammonium chloride (TBACl) in acetonitrile (AN). The procedure is based on two simultaneous processes, namely intercalation, and decalcification. A detailed study of the structure and surface morphology of the produced materials was performed based on a series of microscopic and spectroscopic techniques. The sensing ability of the as-exfoliated samples upon the vapor of several volatile organic compounds (VOCs) was investigated and performed by using impedance spectroscopy. The selectivity analysis of the Ge-enabled sensor was also elucidated while exposure to mixed vapors of methanol and ethanol of various ratio was analyzed. This research provides a new approach to advanced gas sensing integrated with solution-processed few-layer germanene.

## EXPERIMENTAL SECTION

**Characterization methods.** Topological and structural analysis of the exfoliated $H_{edge}$-Ge samples were performed by *Scanning transmission electron microscopy* (Jeol7600F SEM) operating at 30 kV; *Energy-dispersive X-ray analyzer* (acquired with silicon drift detector X-MaxN 80 TS by Oxford Instruments); *Transmission electron microscopy* (EFTEM Jeol 2200 FS microscope) operating at 200 keV; assisted with the selected area electron diffraction technique. The morphology of the samples was also described based on the AFM and XRD

techniques. *Atomic force microscopy* under ambient conditions with a scan rate of 1 Hz and a scan line of 512. The cantilever was is working in a tapping mode with a strain constant of 1.5 kN $m^{-1}$ equipped with a standard silicon tip with a curvature radius lower than 10 nm. *X-ray diffractometry* (Bruker D8) in Bragg−Brentano parafocusing geometry and applying Cu $K_\alpha$ radiation ($\lambda$ = 0.1540598 nm, U = 40 kV, I = 40 mA). *Dynamic Laser Scattering* was used to evaluate the particle size distribution using a Zetasizer ZS90 instrument (Malvern Instruments, Great Britain).

Optical properties of the bulk and exfoliated samples were compared employing Raman and FTIR spectroscopies. *Raman spectroscopy* (Renishaw) is equipped with a charge-coupled device detector and a 532 nm DPSS laser. A single measurement was performed at ambient conditions employing 50× objective, 10 s integration time, and the laser power of 1 mW.

*Fourier Transform Infrared Spectroscopy* was performed on an iS50R FTIR spectrometer (Thermo Scientific, USA). For the measurement samples were drop coated and dried on the gold substrate (200 nm gold film sputtered on the $SiO_2$ wafer).

*X-ray photoelectron spectroscopy* was used to confirm the chemical composition and binding states of bulk and exfoliated samples. XPS spectra were acquired with a monochromatic Al X-ray radiation source (1486.7 eV) and a Phoibos 100 spectrometer (SPECS).

**Chemicals.** The crystals of $CaGe_2$ were grown according to the published procedures and analyses were consistent with previous results.[39] Stoichiometric amount of high-purity germanium (99.999 %) and calcium (99.9 %), corresponding to 10 g of $CaGe_2$ were placed in the 100 ml quartz ampule with an aluminum oxide liner and melt-sealed under a high vacuum

($1 \times 10^{-3}$ Pa). The ampule with the reactive mixture was heated at 1050 °C for 1 hours. This was followed by the slow cooling at the rate of 0.5 °C $min^{-1}$. When the temperature dropped to normal conditions the formed $CaGe_2$ crystals were transferred from the ampule and stored in a glovebox under an inert argon atmosphere.

TBACl was obtained from Sigma–Aldrich. Acetonitrile was obtained from LachNer; it was dried two times for 24 h over molecular sieves. Ethanol, methanol, acetone, isopropyl alcohol, dichloromethane, ethyl acetate, tetrahydrofuran, toluene, and acetic acid were purchased from commercial suppliers such as Sigma–Aldrich, Merck, Penta, Fluorochem and used without further purification.

**Electrochemical exfoliation of edge hydrogenated germanene.** Electrochemical exfoliation of $H_{edge}$-Ge was carried out in the 50 mL electrochemical cell assembled with working (WE) and counter (CE) electrodes. The $CaGe_2$ crystal served as cathode and the WE, and the platinum plate of about 1×2 $cm^2$ size was used as the CE. The non-aqueous solution of TBACl (0.01 M) in AN was employed as the electrolyte. The whole procedure was performed in an oxygen-free atmosphere by purging argon into the electrochemical cell. The exfoliation consists of three stages at different potentials. Starting potential of −1 V was applied to the anode for 2 min to wet the crystal of $CaGe_2$. It follows by the accumulation of the cations (at −2 V for 30 min) in the electrolyte toward WE. The last stage at −2.87 V takes 4–5 hours and combines two simultaneous processes: 1) intercalation of the active ions ($TBA^+$) between the interlayers of $CaGe_2$; 2) decalcification (removal of calcium) by the crystal's interaction with the anionic environment formed of chloride ions. The as-exfoliated material was collected and ultrasonicated for 30 min. Samples were washed in several solvents, namely AN ($H_{edge}$-Ge*)

and 0.01 N acetic acid plus AN ($H_{edge}$-Ge**), and vacuum filtrated. Finally, samples were stored in AN.

**Germanene-enabled vapor sensor: fabrication and test.** Ge-enabled vapor sensors were fabricated by drop-casting of the electrochemically exfoliated germanene, namely $H_{edge}$-Ge* and $H_{edge}$-Ge**. To check the resistivity and behavior of contacts between golden electrodes and the active material the voltampere characteristics were performed. Vapor sensing properties were studied by impedance spectroscopy employing an Autolab PGSTAT204 with the impedance module FRA32M controlled and collected by NOVA 2.1 software. The frequency range was 0.01 Hz to 500 kHz. The amplitude of measurement was 0.01 V. The delay before the measurement was set to 5 min. The measurement was conducted in two-electrode mode on the prepared sensors. The measurement under ambient conditions was employed as a reference.

## RESULTS AND DISCUSSION

**Synthesis and characterization.** Synthesis of few-layer $H_{edge}$-Ge nanosheets was performed by electrochemical exfoliation of $CaGe_2$ crystal in non-aqueous 0.01 M TBACl in AN (see details in the Experimental Section). A platinum plate served as the counter electrode. The whole procedure was carried out in an oxygen-free environment due to continuous purging of argon. The intercalation of the $TBA^+$ ions into $CaGe_2$ interlayers began at a minimum potential of −2.2 V (**Figure S1**), followed by the exfoliation of germanene at −2.87 V. This working potential corresponds to the reduction potential of $Ca^{2+}$.[46] After 4–5 hours of electrochemical exfoliation, the produced germanene flakes were transferred to a vial and ultrasonicated for 30

min. To remove residuals of the TBACl, as well as $CaCl_2$ further washing in AN and 0.01 N acetic acid were performed by vacuum filtration.

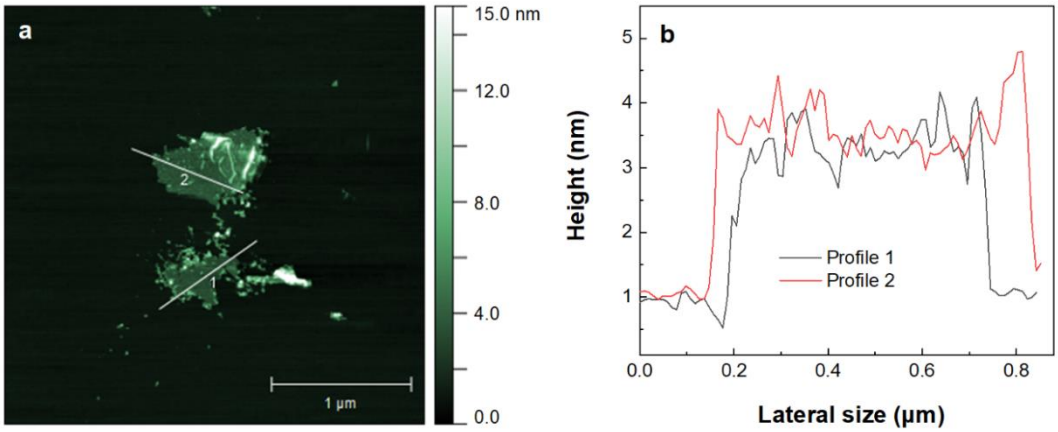


**Figure 1.** Topological characterization of the electrochemically exfoliated few-layer edge-hydrogenated germanene nanosheets: AFM image (a), and corresponding height profiles (b).

A comparative study of the quality and morphology of as-exfoliated germanene was complied by a series of micro- and spectroscopic analysis. The high-resolution STEM images are illustrated in **Figure S2**, both samples $H_{edge}$-Ge* (washed in AN; **Figure S2 a, b**) and $H_{edge}$-Ge** (washed in 0.01 N acetic acid plus AN; **Figure S2 c, d**) are layered flakes with lateral size of up to several micrometers (~1-6 µm). This is consistent with the particle size distribution analysis performed by DLS (**Figure S3**) which shows the presence of the flakes from about 50 nm to several micrometers. Darker sheets on the STEM images correspond to thicker flakes of germanene and are densely self-aggregated with thinner ones. The AFM analysis confirms successful exfoliation of few-layer nanoflakes (**Figure S4**) as well as micrometer size single- and multi-layer germanene (**Figure 1**). Germanene samples are quite homogeneous with a slightly wrinkled surface similar to liquid-processed graphene[47] or phosphorene.[48] The quality of the exfoliated germanene lattice was not affected by the washing procedure.

Detailed morphological insight of the exfoliated $H_{edge}$-Ge was revealed by TEM and SAED (**Figures 2** and **S5**), coupled with TEM-EDX analysis (**Figure S6**). Low-magnification TEM image (**Figure 2 a**) shows well-executed several layers of germanene with lateral size of few micrometers. The corresponding SAED pattern (**Figure 2 b**) exhibited a cubic structure with the germanene plane directions at (002) and (111) and confirmed its layered configuration.

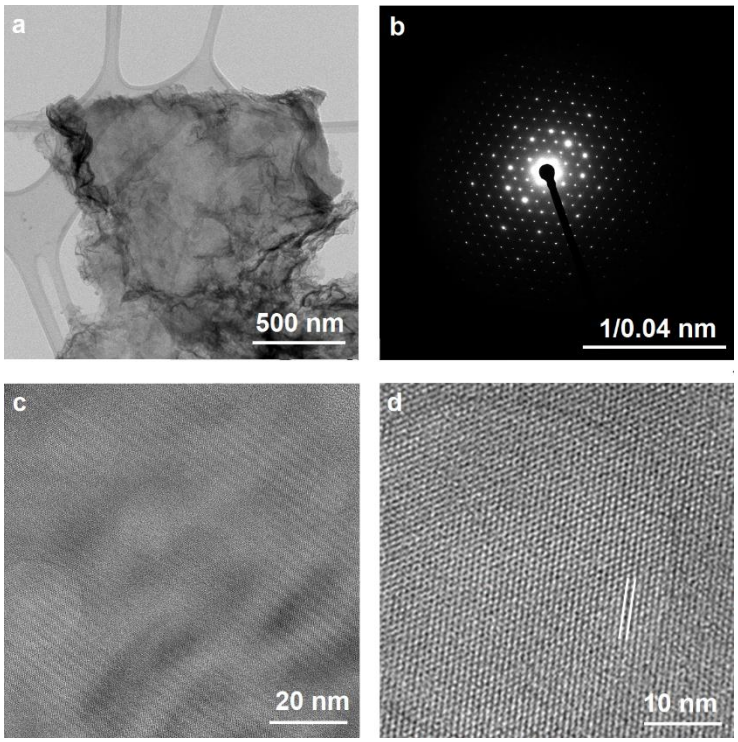


**Figure 2.** TEM analysis of electrochemically exfoliated few-layer edge-hydrogenated germanene in 0.01 M TBACl/AN. High-resolution TEM images at different magnifications (a, c, d) and corresponding SAED pattern revealing a cubic structure (b). The distance between the in-plane Ge atoms is 0.54 nm, marked by two white parallel lines (d).

High-magnification TEM images of $H_{edge}$-Ge in **Figure 2 c, d** showed the in-plane Ge atoms' order in the *y*-direction with an interatomic distance of 0.54 nm. From the TEM-EDX elemental mapping, we confirm the uniform distribution of Ge across the material and traces

of Ca; the concentration of Ca was 6.9% after cleaning samples with AN (**Figure S6 a–c**) and significantly decreased (up to 1.5%) after the additional washing in acetic acid (**Figure S6 d–f**). It has to be pointed out that the structure of germanene sheets becomes silkier as the amount of Ca is reduced.

Structural characterization of the $H_{edge}$-Ge structure was performed by Raman and FTIR spectroscopies (**Figure 3**). Analysis of the Raman spectra revealed the formation of the 2D lattice (**Figure 3 a**) demonstrated by the intense $E_{2g}$ mode (Ge-Ge stretch) at 302 $cm^{-1}$ for both $H_{edge}$-Ge* and $H_{edge}$-Ge** samples. The evident 67 $cm^{-1}$ redshift further confirmed the successful exfoliation of 2D germanene from bulk $CaGe_2$. This is also consistent with the slight redshift of $E_{2g}$ mode compared to the 297 $cm^{-1}$ for crystalline germanium accordingly.[39] The second emerged $A_{1g}$ vibrational mode at 226 $cm^{-1}$ affirms the Ge-H signature which almost disappears after the thorough cleaning of the as-exfoliated samples. The appearance of the $A_{1g}$ mode is caused by a low-level hydrogenation of the germanene.[39] FTIR characteristics are in good agreement with the Raman spectroscopy results and further validate the exfoliation of edge-hydrogenated germanene (**Figure 3 b**). FTIR spectra exhibit two main modes at 808 and 649 $cm^{-1}$ for $H_{egde}$-Ge* and 798 and 679 $cm^{-1}$ for $H_{egde}$-Ge**. The vibrations are assigned as bend (808 and 798 $cm^{-1}$) and wag modes (649 and 679 $cm^{-1}$) that originate from the Ge-$H_2$ bending order from the nearest Ge atoms at the edges within the Ge lattice.[49, 50] For a $H_{edge}$-Ge** sample with a considerably less amount of Ge-H groups, these peaks shift to lower wavelengths. We did not observe the presence of the intense and broad vibrational modes at ~2000 $cm^{-1}$ or in the range 800–1000 $cm^{-1}$ that are the signature for increased hydrogen concentration (Ge-H stretching) or oxidation (Ge-O-Ge and Ge-O vibrations), respectively.[51, 52]

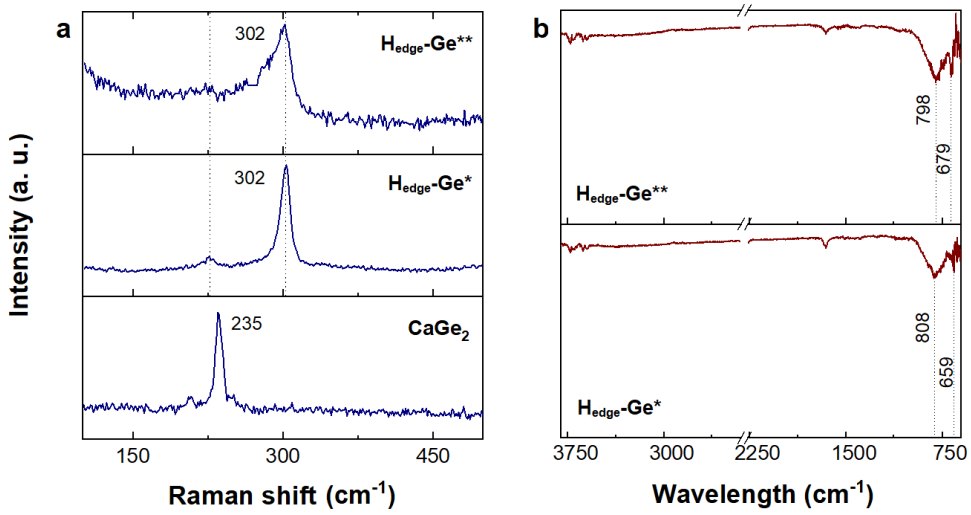


**Figure 3.** Raman (a) and FTIR (b) spectra of the electrochemically exfoliated few-layer edge-hydrogenated germanene, where $H_{edge}$-Ge** – washed in 0.01 N acetic acid and acetonitrile, $H_{edge}$-Ge* – washed in AN only, $CaGe_2$ – initial crystal.

The X-ray powder diffraction was conducted to analyze the structure of the $H_{edge}$-Ge framework and compare it to bulk $CaGe_2$ (**Figure 4a**). The analysis of the XRD pattern of $H_{edge}$-Ge revealed its cubic *Fd-3m* symmetry (PDF card: 04-014-2572) and agreed with the SAED patterns (**Figures 2** and **S5**) and literature.[41] Compared to the original $CaGe_2$ unit cell parameters of $a$ = 3.987 Å, $c$ = 30.583 Å, the unit cell parameters of $H_{edge}$-Ge (with $a$ = 3.621 Å and $c$ = 5.621 Å) demonstrate a slight contraction in the $a$-direction and expansion in the $c$-direction due to the formation of the Ge-$H_2$ bonds between each layer. The low-intensity, broad peak at 13.3° is assigned to the (002) plane of hydrogenated germanene that indicates an interlayer spacing of 3.34 Å. Contrary to previously published results,[53] this spacing is very close to the distance between non-functionalized bilayered germanene[24, 28] and refers to its low-level hydrogenation that occurred at the edges. The peaks at 26.0° and 27.4° scattering angles are assigned to the (100) and (111 ) diffraction reflection, respectively. Their narrower

full-width-at-half-maximum compared to the (002) peak indicates a disorder along the *c*-axis, which is common in layered materials and particularly in buckled germanene.[39] The less intense peak at 45.6° is assigned to the (220) plane reflection of germanium. The presence of Bragg reflections at high angles in the XRD pattern indicates the periodic nature and polycrystallinity of the exfoliated samples. The peaks at 17.2°, 18.3° and 35.4° were attributed to the residuals of $CaGe_2$.

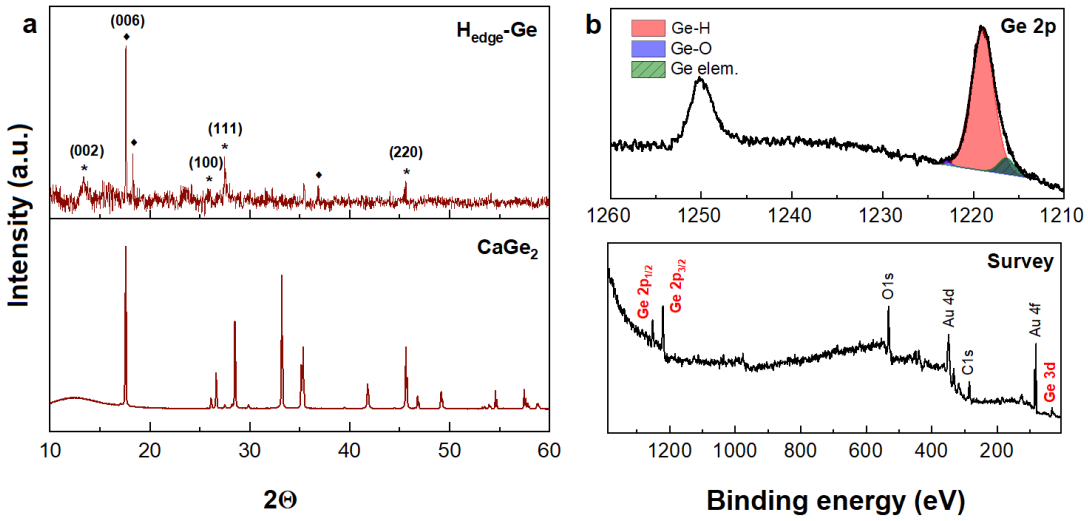


**Figure 4.** Structural analysis of the electrochemically exfoliated few-layer edge-hydrogenated germanene. The XRD spectra (a), where the elemental germanium is marked with the asterisk (*) and residuals of $CaGe_2$ marked as rhomb (♦). The peak at 18.2° scattering angle belongs to $CaGe_2O_5$.[54] The wide survey XPS of $H_{edge}$-Ge and high-resolution spectra of Ge 2p (b).

X-ray photoemission spectroscopy (XPS) was employed to further investigate the bonding configuration of the as-exfoliated $H_{edge}$-Ge. The XPS survey and Ge 2p spectra are demonstrated in **Figure 4 b**. Wide-scan survey spectra confirmed the presence of Ge, C, O as well as Au (samples were drop casted on top of a gold substrate). The values were referenced to an adventitious carbon peak at 284.8 eV, but the absolute values are mainly for illustration

due to sample charging and its semiconducting behaviour.[55] The Ge 2p spectra were fit with three peaks representing elemental germanium at ~1216.1 eV (green area), Ge−H at ~1219.0 eV (red area), and traces of Ge−O at ~1222.8 eV (blue area) that originate from the surface oxidation of germanane. The results demonstrate insignificant oxidation of as-exfoliated germanene and confirmed its surface termination with low-level hydrogenation.

**$H_{edge}$-Ge–enabled vapor sensor.** Efficient detection of volatile organic compounds in human breath or environmental surroundings is significant for healthcare,[56, 57] and ecology.[58] The use of 2D materials has been widely explored for the detection of VOCs and gases,[59] where the intrinsic electrical conductivity[60, 61] (charge transfer, bandgap value) of the materials was considered. For instance, several investigations describe the influence of volatile molecules on 2D surfaces such as metal nanoparticles, metal oxides nanostructures,[62-64] $MoS_2$,[65] $WS_2$,[66] BN,[67] graphene,[60, 68-70] silicene,[71] phosphorene.[72-76] Recently hydrogenated germanene as a 2D graphene analog has been rightly considered for gas sensing yet based on the theoretical study.[10] To date, the only research shows the ability of germanene to detect toxic $NH_3$, $NO_2$, and $SO_2$ gas molecules, in particular $NO_2$ gas, due to its strongest interaction with the germanene (adsorption energy is 273.72 meV) and highest charge transfer value.

After having verified the successful exfoliation of few-layer germanene, planar vapor sensors integrated with $H_{edge}$-Ge* and $H_{edge}$-Ge** were fabricated (see details in the Experimental Section) to evaluate their electrochemical performance to the exposure of the VOCs. The response of the Ge-enabled sensors to the presence of VOCs has been examined by impedance measurements (**Figure 5** and **S**8). The sensors have been exposed to concentrated ethanol (EtOH), methanol (MeOH), acetone, isopropyl alcohol (IPA),

acetonitrile, dichloromethane, ethyl acetate, tetrahydrofuran, and toluene. Initial electrical resistivity of the sensors based on $H_{edge}$-Ge* and $H_{edge}$-Ge** were 0.24 and 0.80 kΩ, correspondingly, and has been stable after the multiple tests. It has been demonstrated that both sensors are sensitive to the presence of EtOH, MeOH, IPA, and acetone (**Figures 5 a**, **S7 a**). In addition, the electrical resistivity increases noteworthily after the sensors are placed in the saturated vapors of the mentioned VOCs. (**Figures 5 b**, **S7b**).

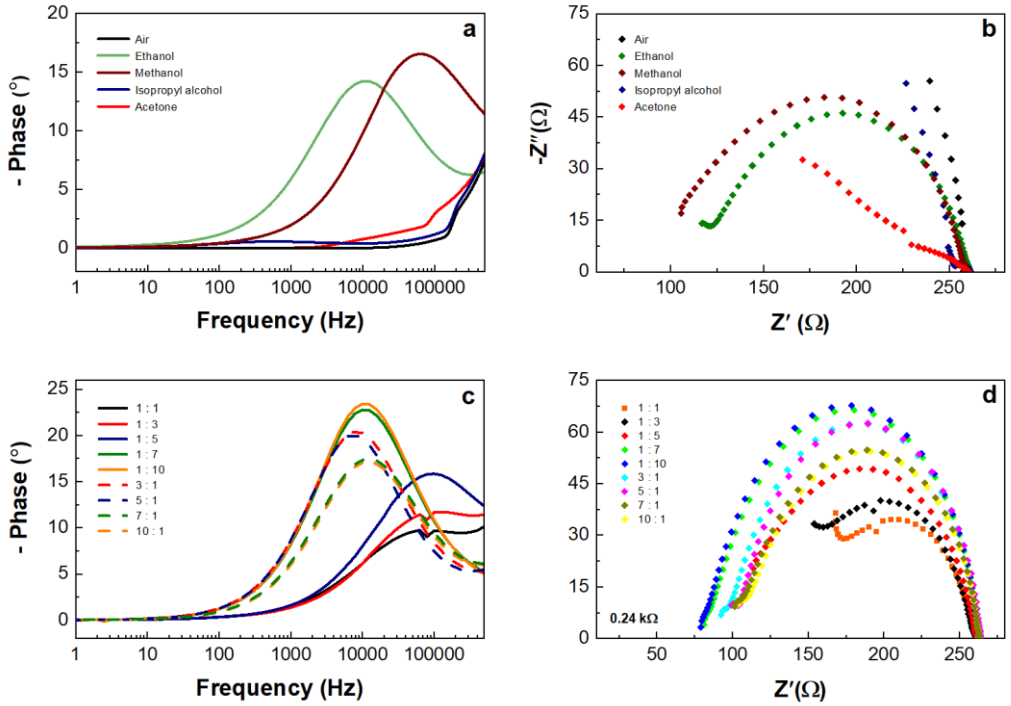


**Figure 5.** $H_{edge}$-Ge**-based vapor sensor characterization: Bode (a, c) and corresponding Nyquist diagrams (b, d). The initial resistivity of the germanene-based gas sensor is about 0.24 kΩ.

The sensitivity analysis of the Ge-based sensor is represented by Bode diagrams which exhibit the frequency and phase shifts of the peak maximum upon the adsorption of the VOCs (**Tables S1** and **S2**). The impedance phase spectra show two prominent peaks at the resonance frequency of about 64 and 60 kHz ($H_{edge}$-Ge*-based sensor) as well as 5 and 1 kHz ($H_{edge}$-Ge**-

based sensor) in presence of MeOH and EtOH vapors, respectively. The phase shift at the peak maximum at approximately 16° and 14° ($H_{edge}$-Ge*–based sensor), as well as 12° and 18° ($H_{edge}$-Ge**–based sensor) has confirmed the sensitivity of both sensors towards MeOH and EtOH. The less intense response upon exposure to IPA and acetone was recorded for both sensors although with the stronger sensitivity of $H_{edge}$-Ge**. The results indicate that Ge-based sensors demonstrate specific sensitivity to MeOH and EtOH caused by their highest polarity and thus strongest interaction with germanene surface.

Additionally, the selectivity of the Ge-based sensors toward methanol over ethanol was evaluated by using a mixture of concentrated solutions in the following ratio of EtOH to MeOH such as 1:1, 1:3, 1:5, 1:7, 1:10, and vice versa (**Tables S3** and **S4**). As shown in **Figure 5 c**, the frequency of the peak maximum for $H_{edge}$-Ge*–based sensor is blueshifted when MeOH predominates and redshifted when EtOH predominates. Based on the Nyquist diagrams (**Figure 5 d**), the phase maximum increases from approximately 10° to 23° with the higher concentration of MeOH in the solution and, consequently, decreases from 23° to 17° when the amount of EtOH prevails. A similar dependence of the frequency and phase of the peak maximum is observed for the sensor integrated with $H_{edge}$-Ge** (**Figure S8**). The increased electrical resistance under the MeOH vapors and decreased under the EtOH vapors is due to the better affinity of the Ge-based electrode toward the less polar but more symmetric MeOH.

## CONCLUSIONS

In conclusion, we have presented the electrochemical exfoliation of few-layer germanene with a low level of hydrogenation for the first time. We have showed that the exfoliation is based on two simultaneous processes, namely decalcification (Ca deintercalation) and intercalation

(insertion of $TBA^+$ cations). Based on a series of analyses we have confirmed the edge-hydrogenated form of germanene and its cubic structure. We have demonstrated a germanene-enabled vapor sensor detecting several organics such as methanol, ethanol, isopropyl alcohol, and acetone. Furthermore, we have shown the selectivity of the germanene-based sensor to methanol over ethanol; the sensor exhibits an increase of the electrical resistance in the vapors where methanol predominates. Overall, the noticeable changes in the electrical resistance will help to distinguish between the volatile organic compounds. This research is highly beneficial for the top-down synthesis of emerging monoelemental 2D materials and their great potential for gas sensing.

AUTHOR INFORMATION

**Corresponding Authors**

*Evgeniya Kovalska

Ievgeniia.Kovalska@vscht.cz; evgeniya.kovalska.ua@gmail.com

*Zdenek Sofer

soferz@vscht.cz

## REFERENCES

1. Ledina, M. A.; Bui, N.; Liang, X.; Kim, Y. G.; Jung, J.; Perdue, B.; Tsang, C.; Drnec, J.; Carlà, F.; Soriaga, M. P.; Reber, T. J.; Stickney, J. L., Electrochemical Formation of Germanene: pH 4.5. Journal of The Electrochemical Society 2017, 164 (7), D469-D477.

2. Cahangirov, S.; Topsakal, M.; Aktürk, E.; Şahin, H.; Ciraci, S., Two- and One-Dimensional Honeycomb Structures of Silicon and Germanium. Physical Review Letters 2009, 102 (23), 236804.

3. Liu, C.-C.; Feng, W.; Yao, Y., Quantum Spin Hall Effect in Silicene and Two-Dimensional Germanium. Physical Review Letters 2011, 107 (7), 076802.

4. Zhuang, J.; Liu, C.; Zhou, Z.; Casillas, G.; Feng, H.; Xu, X.; Wang, J.; Hao, W.; Wang, X.; Dou, S. X.; Hu, Z.; Du, Y., Dirac Signature in Germanene on Semiconducting Substrate. Advanced Science 2018, 5 (7), 1800207.

5. Ni, Z.; Liu, Q.; Tang, K.; Zheng, J.; Zhou, J.; Qin, R.; Gao, Z.; Yu, D.; Lu, J., Tunable Bandgap in Silicene and Germanene. Nano Letters 2012, 12 (1), 113-118.

6. Liu, G.; Luo, W. W.; Wang, X.; Lei, X. L.; Xu, B.; Ouyang, C. Y.; Liu, S. B., Tuning the electronic properties of germanene by molecular adsorption and under an external electric field. Journal of Materials Chemistry C 2018, 6 (22), 5937-5948.

7. Liu, N.; Qiao, H.; Xu, K.; Xi, Y.; Ren, L.; Cheng, N.; Cui, D.; Qi, X.; Xu, X.; Hao, W.; Dou, S. X.; Du, Y., Hydrogen Terminated Germanene for a Robust Self-Powered Flexible Photoelectrochemical Photodetector. Small 2020, 16 (23), 2000283.

8. Li, C.; Kang, J.; Xie, J.; Wang, Y.; Zhou, L.; Hu, H.; Li, X.; He, J.; Wang, B.; Zhang, H., Two-dimensional monoelemental germanene nanosheets: facile preparation and optoelectronic applications. Journal of Materials Chemistry C 2020, 8 (46), 16318-16325.

9. Amamou, W.; Odenthal, P. M.; Bushong, E. J.; O'Hara, D. J.; Kelly Luo, Y.; van Baren, J.; Pinchuk, I.; Wu, Y.; Ahmed, A. S.; Katoch, J.; Bockrath, M. W.; Tom, H. W. K.; Goldberger, J. E.; Kawakami, R. K., Large area epitaxial germanane for electronic devices. 2D Materials 2015, 2 (3), 035012.

10. Gupta, S. K.; Singh, D.; Rajput, K.; Sonvane, Y., Germanene: a new electronic gas sensing material. RSC Advances 2016, 6 (104), 102264-102271.

11. Xia, W.; Hu, W.; Li, Z.; Yang, J., A first-principles study of gas adsorption on germanene. Physical Chemistry Chemical Physics 2014, 16 (41), 22495-22498.

12. Hussain, T.; Kaewmaraya, T.; Chakraborty, S.; Vovusha, H.; Amornkitbamrung, V.; Ahuja, R., Defected and Functionalized Germanene-based Nanosensors under Sulfur Comprising Gas Exposure. ACS Sensors 2018, 3 (4), 867-874.

13. Zhu, J.; Chroneos, A.; Schwingenschlögl, U., Silicene/germanene on MgX2 (X = Cl, Br, and I) for Li-ion battery applications. Nanoscale 2016, 8 (13), 7272-7277.

14. Serino, A. C.; Ko, J. S.; Yeung, M. T.; Schwartz, J. J.; Kang, C. B.; Tolbert, S. H.; Kaner, R. B.; Dunn, B. S.; Weiss, P. S., Lithium-Ion Insertion Properties of Solution-Exfoliated Germanane. ACS Nano 2017, 11 (8), 7995-8001.

15. Mortazavi, B.; Dianat, A.; Cuniberti, G.; Rabczuk, T., Application of silicene, germanene and stanene for Na or Li ion storage: A theoretical investigation. Electrochimica Acta 2016, 213, 865-870.

16. Giousis, T.; Potsi, G.; Kouloumpis, A.; Spyrou, K.; Georgantas, Y.; Chalmpes, N.; Dimos, K.; Antoniou, M.-K.; Papavassiliou, G.; Bourlinos, A. B.; Kim, H. J.; Wadi, V. K. S.; Alhassan, S.; Ahmadi, M.; Kooi, B. J.; Blake, G.; Balazs, D. M.; Loi, M. A.; Gournis, D.; Rudolf, P., Synthesis of 2D Germanane (GeH): a New, Fast, and Facile Approach. Angewandte Chemie International Edition 2021, 60 (1), 360-365.

17. Liu, Z.; Lou, Z.; Li, Z.; Wang, G.; Wang, Z.; Liu, Y.; Huang, B.; Xia, S.; Qin, X.; Zhang, X.; Dai, Y., GeH: a novel material as a visible-light driven photocatalyst for hydrogen evolution. Chemical Communications 2014, 50 (75), 11046-11048.

18. Chegel, R.; Behzad, S., Tunable Electronic, Optical, and Thermal Properties of two- dimensional Germanene via an external electric field. Scientific Reports 2020, 10 (1), 704.

19. Kaloni, T. P.; Schwingenschlögl, U., Stability of germanene under tensile strain. Chemical Physics Letters 2013, 583, 137-140.

20. Jiang, S.; Butler, S.; Bianco, E.; Restrepo, O. D.; Windl, W.; Goldberger, J. E., Improving the stability and optical properties of germanane via one-step covalent methyl-termination. Nature Communications 2014, 5 (1), 3389.

21. Jiang, S.; Krymowski, K.; Asel, T.; Arguilla, M. Q.; Cultrara, N. D.; Yanchenko, E.; Yang, X.; Brillson, L. J.; Windl, W.; Goldberger, J. E., Tailoring the Electronic Structure of Covalently Functionalized Germanane via the Interplay of Ligand Strain and Electronegativity. Chemistry of Materials 2016, 28 (21), 8071-8077.

22. Padilha, J. E.; Abdalla, L. B.; da Silva, A. J. R.; Fazzio, A., Fully and partially iodinated germanane as a platform for the observation of the quantum spin Hall effect. Physical Review B 2016, 93 (4), 045135.

23. Dimoulas, A., Silicene and germanene: Silicon and germanium in the “flatland”. Microelectronic Engineering 2015, 131, 68-78.

24. Dávila, M. E.; Xian, L.; Cahangirov, S.; Rubio, A.; Le Lay, G., Germanene: a novel two-dimensional germanium allotrope akin to graphene and silicene. New Journal of Physics 2014, 16 (9), 095002.

25. Bampoulis, P.; Zhang, L.; Safaei, A. v.; van Gastel, R.; Poelsema, B.; Zandvliet, H. J. W., Germanene termination of $Ge_2Pt$ crystals on Ge (110). Journal of physics: Condensed matter 2014, 26 (44), 442001.

26. d’Acapito, F.; Torrengo, S.; Xenogiannopoulou, E.; Tsipas, P.; Velasco, J. M.; Tsoutsou, D.; Dimoulas, A., Evidence for Germanene growth on epitaxial hexagonal (h)-AlN on Ag (111). Journal of Physics: Condensed Matter 2016, 28 (4), 045002.

27. Derivaz, M.; Dentel, D.; Stephan, R.; Hanf, M.-C.; Mehdaoui, A.; Sonnet, P.; Pirri, C., Continuous Germanene Layer on Al (111). Nano Letters 2015, 15 (4), 2510-2516.

28. Tsai, H.-S.; Chen, Y.-Z.; Medina, H.; Su, T.-Y.; Chou, T.-S.; Chen, Y.-H.; Chueh, Y.-L.; Liang, J.-H., Direct formation of large-scale multi-layered germanene on Si substrate. Physical Chemistry Chemical Physics 2015, 17 (33), 21389-21393.

29. Persichetti, L.; Jardali, F.; Vach, H.; Sgarlata, A.; Berbezier, I.; De Crescenzi, M.; Balzarotti, A., van der Waals Heteroepitaxy of Germanene Islands on Graphite. The Journal of Physical Chemistry Letters 2016, 7 (16), 3246-3251.

30. Zhang, L.; Bampoulis, P.; Rudenko, A. N.; Yao, Q.; van Houselt, A.; Poelsema, B.; Katsnelson, M. I.; Zandvliet, H. J. W., Structural and Electronic Properties of Germanene on $MoS_2$. Physical Review Letters 2016, 116 (25), 256804.

31. Bui, N. N.; Ledina, M.; Reber, T. J.; Jung, J.; Stickney, J. L., Electrochemical Scanning Tunneling Microscopic Study of the Potential Dependence of Germanene Growth on Au (111) at pH 9.0. ACS Nano 2017, 11 (9), 9481-9489.

32. Fahrenkrug, E.; Gu, J.; Jeon, S.; Veneman, P. A.; Goldman, R. S.; Maldonado, S., Room-Temperature Epitaxial Electrodeposition of Single-Crystalline Germanium Nanowires at the Wafer Scale from an Aqueous Solution. Nano Letters 2014, 14 (2), 847-852.

33. Liang, X.; Kim, Y.-G.; Gebergziabiher, D. K.; Stickney, J. L., Aqueous Electrodeposition of Ge Monolayers. Langmuir 2010, 26 (4), 2877-2884.

34. Jung, J.; Bui, N. N.; Shen, S.; Reber, T. J.; Brezner, J. M.; Mubeen, S.; Stickney, J. L., In Situ Surface-Enhanced Raman Spectroscopic Studies of Electrochemically Formed Germanene. The Journal of Physical Chemistry C 2018, 122 (27), 15696-15705.

35. Szekely, G., Electrodeposition of germanium. Journal of The Electrochemical Society 1951, 98 (8), 318.

36. Endres, F.; Zein El Abedin, S., Nanoscale electrodeposition of germanium on Au (111) from an ionic liquid: an in situ STM study of phase formation Part I. Ge from $GeBr_4$. Physical Chemistry Chemical Physics 2002, 4 (9), 1640-1648.

37. Endres, F., Electrodeposition of a thin germanium film on gold from a room temperature ionic liquid. Physical Chemistry Chemical Physics 2001, 3 (15), 3165-3174.

38. Cultrara, N. D.; Wang, Y.; Arguilla, M. Q.; Scudder, M. R.; Jiang, S.; Windl, W.; Bobev, S.; Goldberger, J. E., Synthesis of 1T, 2H, and 6R Germanane Polytypes. Chemistry of Materials 2018, 30 (4), 1335-1343.

39. Bianco, E.; Butler, S.; Jiang, S.; Restrepo, O. D.; Windl, W.; Goldberger, J. E., Stability and Exfoliation of Germanane: A Germanium Graphane Analogue. ACS Nano 2013, 7 (5), 4414-4421.

40. Koski, K. J.; Cui, Y., The new skinny in two-dimensional nanomaterials. Acs Nano 2013, 7 (5), 3739-3743.

41. Sahoo, N. G.; Esteves, R. J.; Punetha, V. D.; Pestov, D.; Arachchige, I. U.; Jr., J. T. M., Schottky diodes from 2D germanane. Applied Physics Letters 2016, 109 (2), 023507.

42. Ang, W. L.; Sturala, J.; Antonatos, N.; Sofer, Z.; Bonanni, A., Effect of surface chemistry on bio-conjugation and bio-recognition abilities of 2D germanene materials. Nanoscale 2021, 13 (3), 1893-1903.

43. Saxena, V.; Atsumi, N.; Shimura, Y.; Tatsuoka, H., Synthesis of Ge-based nanosheet bundles using calcium germanides as templates in $IP_6$ aqueous solution. Japanese Journal of Applied Physics 2020, 59 (SG), SGGK08.

44. Yaokawa, R.; Ohsuna, T.; Hayasaka, Y.; Nakano, H., Multilayer Germanenes Formed in Zintl-Phase $CaGe_2$ by Fluoride Diffusion. ChemistrySelect 2016, 1 (17), 5579-5583.

45. Glavinović, M.; Krause, M.; Yang, L.; McLeod, J. A.; Liu, L.; Baines, K. M.; Friščić, T.; Lumb, J.-P., A chlorine-free protocol for processing germanium. Science Advances 2017, 3 (5), e1700149.

46. Atkins, P.; Overton, T., Shriver and Atkins' inorganic chemistry. Oxford University Press, USA: 2010.

47. Achee, T. C.; Sun, W.; Hope, J. T.; Quitzau, S. G.; Sweeney, C. B.; Shah, S. A.; Habib, T.; Green, M. J., High-yield scalable graphene nanosheet production from compressed graphite using electrochemical exfoliation. Scientific Reports 2018, 8 (1), 14525.

48. Kovalska, E.; Luxa, J.; Hartman, T.; Antonatos, N.; Shaban, P.; Oparin, E.; Zhukova, M.; Sofer, Z., Non-aqueous solution-processed phosphorene by controlled low-potential electrochemical exfoliation and thin film preparation. Nanoscale 2020, 12 (4), 2638-2647.

49. Bermejo, D.; Cardona, M., Infrared absorption in hydrogenated amorphous and crystallized germanium. Journal of Non-Crystalline Solids 1979, 32 (1), 421-430.

50. Cardona, M., Vibrational Spectra of Hydrogen in Silicon and Germanium. physica status solidi (b) 1983, 118 (2), 463-481.

51. Sturala, J.; Luxa, J.; Matějková, S.; Sofer, Z.; Pumera, M., Germanane synthesis with simultaneous covalent functionalization: towards highly functionalized fluorescent germananes. Nanoscale 2019, 11 (41), 19327-19333.

52. Rivillon, S.; Chabal, Y. J.; Amy, F.; Kahn, A., Hydrogen passivation of germanium (100) surface using wet chemical preparation. Applied Physics Letters 2005, 87 (25), 253101.

53. Sturala, J.; Luxa, J.; Matějková, S.; Plutnar, J.; Hartman, T.; Pumera, M.; Sofer, Z., Exfoliation of Calcium Germanide by Alkyl Halides. Chemistry of Materials 2019, 31 (24), 10126-10134.

54. https://www.materialsproject.org/materials/mp-3707/

55. Greczynski, G.; Hultman, L., X-ray photoelectron spectroscopy: Towards reliable binding energy referencing. Progress in Materials Science 2020, 107, 100591.

56. Bartzis, J.; Wolkoff, P.; Stranger, M.; Efthimiou, G.; Tolis, E. I.; Maes, F.; Nørgaard, A. W.; Ventura, G.; Kalimeri, K. K.; Goelen, E.; Fernandes, O., On organic emissions testing from indoor consumer products' use. Journal of Hazardous Materials 2015, 285, 37-45.

57. André, L.; Desbois, N.; Gros, C. P.; Brandès, S., Porous materials applied to biomarker sensing in exhaled breath for monitoring and detecting non-invasive pathologies. Dalton Transactions 2020, 49 (43), 15161-15170.

58. Salthammer, T., Very volatile organic compounds: an understudied class of indoor air pollutants. Indoor Air 2016, 26 (1), 25-38.

59. Broza, Y. Y.; Haick, H., Nanomaterial-based sensors for detection of disease by volatile organic compounds. Nanomedicine 2013, 8 (5), 785-806.

60. Kovalska, E.; Lesongeur, P.; Hogan, B. T.; Baldycheva, A., Multi-layer graphene as a selective detector for future lung cancer biosensing platforms. Nanoscale 2019, 11 (5), 2476-2483.

61. Kovalska, E.; Luxa, J.; Melle-Franco, M.; Wu, B.; Marek, I.; Roy, P. K.; Marvan, P.; Sofer, Z., Single-Step Synthesis of Platinoid-Decorated Phosphorene: Perspectives for Catalysis, Gas Sensing, and Energy Storage. ACS Applied Materials & Interfaces 2020, 12 (45), 50516-50526.

62. Mirzaei, A.; Leonardi, S.; Neri, G., Detection of hazardous volatile organic compounds (VOCs) by metal oxide nanostructures-based gas sensors: A review. Ceramics international 2016, 42 (14), 15119-15141.

63. Dral, A. P.; Johan, E., 2D metal oxide nanoflakes for sensing applications: Review and perspective. Sensors and Actuators B: Chemical 2018, 272, 369-392.

64. Zhang, Z.; Zou, X.; Xu, L.; Liao, L.; Liu, W.; Ho, J.; Xiao, X.; Jiang, C.; Li, J., Hydrogen gas sensor based on metal oxide nanoparticles decorated graphene transistor. Nanoscale 2015, 7 (22), 10078-10084.

65. Zhao, S.; Xue, J.; Kang, W., Gas adsorption on $MoS_2$ monolayer from first-principles calculations. Chemical Physics Letters 2014, 595-596, 35-42.

66. Bui, V. Q.; Pham, T.-T.; Le, D. A.; Thi, C. M.; Le, H. M., A first-principles investigation of various gas (CO, $H_2O$, NO, and $O_2$) absorptions on a $WS_2$ monolayer: stability and electronic properties. Journal of Physics: Condensed Matter 2015, 27 (30), 305005.

67. Bhat, C.; BrajPuriya, R.; Mishra, P.; Jain, S. K.; Srivastava, A. In Electronic and transport properties of BN sheet on adsorption of amine ($NH_2$) group, 2014 9th International Conference on Industrial and Information Systems (ICIIS), 15-17 Dec. 2014; 2014; pp 1-4.

68. Tripathi, K. M.; Kim, T.; Losic, D.; Tung, T. T., Recent advances in engineered graphene and composites for detection of volatile organic compounds (VOCs) and non-invasive diseases diagnosis. Carbon 2016, 110, 97-129.

69. Konvalina, G.; Haick, H., Sensors for Breath Testing: From Nanomaterials to Comprehensive Disease Detection. Accounts of Chemical Research 2014, 47 (1), 66-76.

70. Hussain, T.; Sajjad, M.; Singh, D.; Bae, H.; Lee, H.; Larsson, J. A.; Ahuja, R.; Karton, A., Sensing of volatile organic compounds on two-dimensional nitrogenated holey graphene, graphdiyne, and their heterostructure. Carbon 2020, 163, 213-223.

71. Chandiramouli, R.; Srivastava, A.; Nagarajan, V., NO adsorption studies on silicene nanosheet: DFT investigation. Applied Surface Science 2015, 351, 662-672.

72. Nagarajan, V.; Chandiramouli, R., Nitrogen dioxide and ammonia gas molecules interaction studies on phosphorene nanosheet---a DFT investigation. arXiv preprint arXiv:1903.11500 2019.

73. Safari, F.; Moradinasab, M.; Fathipour, M.; Kosina, H., Adsorption of the $NH_3$, NO, $NO_2$, $CO_2$, and CO gas molecules on blue phosphorene: A first-principles study. Applied Surface Science 2019, 464, 153-161.

74. Bhuvaneswari, R.; Chandiramouli, R., First-principles investigation on detection of phosgene gas molecules using phosphorene nanosheet device. Chemical Physics Letters 2019, 717, 99-106.

75. Snehha, P.; Nagarajan, V.; Chandiramouli, R., Interaction Behavior of Cyanogen Fluoride and Chloride Gas Molecules on Red Phosphorene Nanosheet: A DFT Study. Journal of Inorganic and Organometallic Polymers and Materials 2019, 29 (3), 954-963.

76. Sun, S.; Hussain, T.; Zhang, W.; Karton, A., Blue phosphorene monolayers as potential nano sensors for volatile organic compounds under point defects. Applied Surface Science 2019, 486, 52-57.